Sinehbaghizadeh, S., Saptoro, A., Naeiji, P., Tiong, A. N. T., Mohammadi, A. H. (2022): Insights into the synergistic effects of metal particles (Ag, Cu, and Fe) and urea on CO2 clathrate hydrate growth using molecular dynamics simulations. - Chemical Engineering Science, 264, 118194.

https://doi.org/10.1016/j.ces.2022.118194

Insights into the synergistic effects of metal particles (Ag, Cu, and Fe) and urea on CO_2 clathrate hydrate growth using molecular dynamics simulations

Saeed Sinehbaghizadeh [a*], Agus Saptoro [a*], Parisa Naeiji [b],

Angnes Tiong Ngieng Tze [a], Amir H. Mohammadi [c]

[a] Department of Chemical and Energy Engineering, Curtin University, CDT 250, Miri 98009, Sarawak, Malaysia

[b] GFZ German Research Centre for Geosciences, Telegrafenberg, 14473 Potsdam, Germany

[c] Discipline of Chemical Engineering, School of Engineering, University of KwaZulu-Natal, Howard College Campus, King George V Avenue, Durban 4041, South Africa

* Corresponding authors, E-mail addresses:

Agus Saptoro, agus.saptoro@curtin.edu.my

Saeed Sinehbaghizadeh, s.baghizadeh@postgrad.curtin.edu.my

Abstract

A variety of industrial applications of hydrate-based CO_2 capture and utilization technologies are hindered by the complex and slow hydrate formation; however, improving CO_2 hydrate formation kinetics can be facilitated by adding the accelerators (promoters). In this regard, understanding the promotion mechanisms of these compounds on the hydrate formation at the molecular level would assist in either establishing feasible processes or finding more efficient promoters. In this work, CO_2 hydrate growth and formation in the presence of hybrid metal particles (Ag, Cu, and Fe) and urea molecule has been explored through molecular dynamics (MD) simulation at below and above water freezing point. Different criteria were used to characterize and analyse the CO_2 hydrate formation kinetics. The outcomes reveal that, although the mixture of Cu, Ag, and Fe metal particles has positive effects on the rate of hydrate formation above the ice point, the mixture of Cu, Fe, and urea (without the inclusion of Ag) in comparison with the other investigated systems, possesses the highest promotion effect on the clathrate hydrate growth rate. This combination of metal particles creates various functions in the solution phase adjacent to the hydrate surface. The metal particles and urea could promote the formation of new cages at the hydrate-solution boundary by decreasing the heat and mass transport resistances of CO_2 in water. In addition, the improvement of combined metal particles and urea under water freezing was found to be less substantial. However, the behaviours of combined metal particles without urea at different thermodynamic conditions are quite dissimilar.

Keywords: CO_2 hydrate; Kinetic promoter; Molecular dynamics (MD) simulations; Metal particles, urea molecule; CO_2 capture; CO_2 utilization.

1. Introduction

Many industrial countries are committed to controlling the emission of greenhouse gases, more specifically CO_2. Cutting down the generated CO_2 by optimizing the processes involved in manufacturing divisions, capturing CO_2, and developing CO_2 utilization/ conversion technologies to produce valuable products could sequentially be the most immediate pathway. Although the methods such as adsorption (Ayittey et al., 2020b, 2020a; Dhoke et al., 2021; Saptoro and Huo, 2013; Zhu et al., 2021), absorption (Ayittey et al., 2021; Hafizi et al., 2021; Jiang et al., 2021), membrane (Senatore et al., 2021; Wu et al., 2021; Zhang et al., 2021), and cryogenic (Cann et al., 2021; Machida et al., 2021) for capturing CO_2 from the emitted gas mixtures have been proposed, gas hydrate crystallization would also be a novel technique for CO_2 separation from the flue gas (Gambelli et al., 2021), fuel gas (Muromachi, 2021), landfill gas (Xu et al., 2019) as well as syngas (Rezaei et al., 2022). Gas hydrate technologies according to the U.S. Department of Energy was known as a promising method for CO_2 capture and storage (Elwell and Grant, 2006). Estimations suggest that 1 m^3 of hydrate can store 170 m^3 of gas at standard conditions (Strobel et al., 2007). Moreover, the separated CO_2 can be utilized or sequestered by other hydrate-based applications e.g. refrigeration systems (Xie et al., 2019), seawater desalination (Babu et al., 2018), fruits juice concentration (Rudolph et al., 2021), and gas storage applications (Jokar et al., 2021). This method can also be used for exploiting CH_4 from deposited hydrate in oceans or permafrost regions and coincide with sequestering CO_2 in the geological sites (Zhang et al., 2017).

Clathrate hydrates are composed of water and suitable size gas molecules entrapped in the cages which are formed by the network of hydrogen-bonded water molecules. Under prevailing thermodynamic conditions and with considering the molecular diameter, and chemical properties of guest molecules, three different clathrate structures of hydrates (sI, sII, and sH) can be formed.

Among the different hydrate guests, the CO_2 molecule at moderated formation pressure by contributing to the hydrate phase can generate sI of the clathrate (Sloan and Koh, 2008). Although the issue of hydrate formation pressure by adding the second guest namely large molecular liquid hydrocarbons to the water phase can be reduced (Sinehbaghizadeh et al., 2019b, 2019a, 2018, 2017), the rate of CO_2 hydrate formation from a kinetic point of view is inappreciable which hinders the hydrate-based processes toward being industrialized. Many investigations have been conducted to discover qualified promotion agents. A good example of this is the addition of nanoparticles which help to enhance the mass transfer at the interface of solid and solution by creating numerous nucleation sites. Evidence suggests the influence of nanoparticles on clathrate hydrate growth is highly complicated and dependent on a variety of influencing factors. Also, the surface functional groups of nanoparticles may determine the promoter or inhibitor effects (Liu et al., 2020; Yu et al., 2016; Zhou et al., 2014). According to an investigation of the kinetics of hydrate formation in contact with Cu, and Ag nanoparticles, it was found that the effects of Cu and Ag nanoparticles are intermediate and insignificant respectively. Also, nanoparticles with high specific areas may enhance the mass transfer and improve gas consumption by activating the interfacial area (Adibi et al., 2020; Said et al., 2016). The equilibrium formation condition for different additives is also unique. For example, the best concentration and condition for Fe_3O_4 nanoparticles in contact with the magnetic field were found to be 0.15 wt% at 4 MPa and 274 K respectively (Firoozabadi et al., 2018). Furthermore, the inclusion of the secondary or a couple of substances to the primary solution system may manifold the positive impressions of additives. There are several organic and environmentally harmless components that have been acknowledged as thermodynamic inhibitors but simultaneously strong kinetic promoters. As a low-toxic biological metabolite, the addition of urea can be regarded as a thermodynamic inhibitor for CO_2

hydrate (Gong et al., 2022; Muromachi et al., 2015), however, the kinetic effects of urea on CO_2 hydrates were found to be substantial and in the macroscopic scale, urea kinetically acts as a promoter for clathrate hydrate of CO_2. It was reported that at 2.7 MPa and 278K, the inclusion of urea can halve the induction time of CO_2 hydrate during crystallization (Chen, C.H. Ho, 2017). Through experimental investigations such as X-ray diffraction (XRD) and Raman or NMR spectroscopy, the distribution of guest molecules in the cages, as well as the crystalline identification of structures can be studied. However, it is difficult to determine the relationship between the nature of components in the system and the process of crystallization at a molecular level as well as initial nanoseconds. To assess and explore the positive and negative aspects of promoters on CO_2 hydrate besides the macroscopic experiments, molecular dynamics (MD) simulations can be perfectly employed. We recently reviewed the role of hydrate promoters and MD frameworks of CO_2 clathrate hydrates in terms of new insights and research findings to elucidate the fundamental properties of CO_2 hydrates at the molecular level (Sinehbaghizadeh et al., 2022b). MD results of CO_2 double and mixed hydrates showed that the type of hydrate promoters can play a determinative role in the stabilization of the clathrate hydrate network (Sinehbaghizadeh et al., 2022a). MD simulation trajectories suggested that urea may appear to mediate the meta-stable amorphous hydrate and modification of solution characteristics for supporting clathrate hydrate formation (Lim et al., 2014). Also, molecular analysis of CO_2 hydrate formation with metal particles (Cu, Fe, and Ag) at various concentrations clarified that such microparticles possess a mixed effect on growth kinetics. Furthermore, the promoting effect of Cu at 1.0 wt% on hydrate growth was found to be higher than either Fe or Ag. Although the effect of Fe particles had a medium promotion, Ag particles were found to be little impact on the growth rate of CO_2 hydrate or even act as an inhibitor (Liu et al., 2021). Moreover, the formation rate can

be attributed to the operating conditions of the system. Through the MD framework, the CO_2 hydrate growth in contact with Ag nanoparticles at 260 K was found to be more rapid than either at 250 K or 270 K. Additionally, Ag additive may facilitate CO_2 dissolution as well as diffusion coefficient by increasing the CO_2 molecular migration from the solution side to the solid-liquid boundary (Mahmoodi et al., 2021).

Although some MD works in the literature have studied the different aspects of CO_2 hydrate formation with promoters, investigations directed toward a better understanding of the synergistic effects of the hydrate promoters from diverse types at the molecular level have mostly remained unexplored and poorly understood. Thus, in this work, the synergistic effects of metal particles and urea on the solution phase in contact with CO_2 sI hydrate were studied. To the best of our knowledge, this is the first investigation that analyses the hybrid addition of these materials on CO_2 hydrate growth via acting at the solid-solution interface. The simulation results of this work can be useful to understand the mechanisms involved in CO_2 hydrate formation in the presence of synergic additives. It is worth mentioning that the interpretation of MD observations may help to accelerate the practical implementations of hydrate-based CO_2 capture and utilization (HBCC/U) systems.

2. Simulation methodology

2.1. Model Setup

The simulation system consists of a crystal layer of CO_2 sI hydrate sandwiched by a solution of CO_2 and water was considered as an initial configuration. The CO_2 hydrate slab was employed as the solid substrate for hydrate growth so that it would help to overcome the time lag of initial nucleation. To build the initial hydrate, a unit cell of sI hydrate with a lattice parameter of 12.03 Å

was adopted (Takeuchi et al., 2013). To generate a 2×2×2 hydrate slab containing 368 water and 64 CO_2 molecules, the sI hydrate unit cell was replicated two times in all directions (24.06 × 24.06 × 24.06 $Å^3$). The CO_2 molecules were located at the centre of both small and large cages. Subsequently, the hydrate slab was allocated in the middle of the mixture of 736 water and 128 CO_2 molecules, yielding a simulation box length of 72 Å in the Z direction. Also, the solution and hydrate substrate were aligned to the X-Y plane (cross-section area) with the same dimension of 24.06 Å. The periodic boundary conditions in all directions were set so that the hydrate substrate model along the X and Y directions could be effectively infinite. To understand the microscopic effects of the combination of metal particles and molecular impacts of urea, the growth of CO_2 hydrates in the presence of such mixtures was evaluated; Table 1 gives the combined additives as well as their concentrations. In addition, the presence of pure Cu metal particles and single urea to make a comparison with mixed additives were also simulated. Each set of the simulation was carried out at two P-T conditions of 2 MPa and 260 K, 3 MPa and 275 K. It is worth noting that the high concentrations of solid metal particles can cause a stronger Brownian motion in the solution. Accordingly, it may increase the activation energy to agglomerate and inhibit orderly intermolecular movements (Liu et al., 2021). Therefore, the low concentrations of these additives in this work were chosen.

Table 1: List of mixed additives and amounts in the water solution.

No.	**Hydrate additive**	**No. of metal atom(s)/ molecule in the solution**				**Content in the solution (wt%)**
		Cu	**Fe**	**Ag**	**Urea**	
1	Pure water	-	-	-	-	-
2	Urea	-	-	-	1	Urea molecule (0.32%)
3	Cu	3	-	-	-	metal particles [Cu (1.01%)]

4	Cu+Ag-(1)	1	-	1	-	metal particles [Cu (0.33%) + Ag (0.56%)]
5	Cu+Fe-(1)	1	1	-	-	metal particles [Cu (0.33%) + Fe (0.29%)]
6	Cu+Ag+Fe-(1)	1	1	1	-	metal particles [Cu (0.33%) + Ag (0.56%) + Fe (0.29%)]
7	Cu+Ag-(2)	2	-	2	-	metal particles [Cu (0.66%) + (Ag (1.12%)]
8	Cu+Ag+Fe-(2)	2	2	2	-	metal particles [Cu (0.66%) + Ag (1.12%) + Fe (0.58%)]
9	Cu+Fe+Urea-(1)	1	1	-	1	metal particles [Cu (0.33%) + Fe (0.29%)] + Urea molecule (0.32%)
10	Cu+Ag+Fe+Urea-(1)	1	1	1	1	metal particles [Cu (0.33%) + Ag (0.56%) + Fe (0.29%)] + Urea molecule (0.32%)

2.2. Computational details

All MD simulations were carried out with the utilization of LAMMPS software, developed by Sandia National Laboratories which is an open-source code (Steve and Paul, 2012). The accuracy of MD simulations is dependent upon the force field and the parameters used to define the interactions in the system. Intramolecular interactions are normally described in the energy terms of deformation and coupling terms between deformations of internal coordinates whereas Intermolecular interactions contain the Lennard-Jones function and the electrostatic term (Frenkel and Smit, 2002). Since the TIP4P/Ice force field has been successfully employed to describe the properties of water during hydrate growth (Maddah et al., 2018; Mahmoodi et al., 2021; Phan et al., 2021), water molecules were simulated by this intermolecular model (Abascal et al., 2005). Moreover, it was previously shown that among the different versions of TIP4P water models, the TIP4P/Ice approach yields better agreement with the CO_2 hydrate experimental results (Míguez et al., 2015). The CO_2 molecules were also modelled using the TraPPE potential model (Eggimann et al., 2014). This force field can quantitatively reproduce the vapor-liquid equilibria (VLE) of the neat/ mixed systems and create a good balance between dispersive and electrostatic (quadrupole-

quadrupole) interactions. To model the interactions of urea molecules, the potential approach proposed by Kallies was utilized (Kallies, 2002). Using this force field, the effects of urea on the structure of water and the properties in terms of the extent of the hydrogen-bond network, the interaction energy, and radial profiles of excess coordination numbers have been successfully analysed (Idrissi et al., 2010; Wang et al., 2021). In addition, the Lennard-Jones potential was applied to describe the behaviour of metal particles in the simulated systems. Due to the limitations of computer hardware, single atoms for Cu, Fe, and Ag metal particles instead of metal clusters were considered to reduce the number of calculations (Liu et al., 2021). In the system containing Cu, Fe, and Ag additives, the metal particles were uniformly distributed in the solution. The Lennard-Jones parameters between unlike atoms were calculated from the geometric combination rule [$\varepsilon_{ij}=(\varepsilon_{ii}.\varepsilon_{jj})^{1/2}$ and $\sigma_{ij}=(\sigma_{ii}.\sigma_{jj})^{1/2}$]. The long-range Coulomb interactions were calculated with a cut-off of 12 Å and calculated using the "pppm" algorithm (Hockney and Eastwood, 2021). To constrain the rigidity of water molecules, the Shake algorithm was utilized (Ryckaert et al., 1977). By applying the conjugate gradient algorithm, the energy minimization before each simulation was carried out. The initial configurations at the simulation temperatures were then conducted in the *NVT* canonical ensemble for 40 ps. This step was subsequently followed by performing *NPT* ensemble for at least 150 ns by Nose-Hoover thermostat and barostat with the time step of 1fs. Implementing *NPT* ensemble can be useful for investigating the hydrate growth phenomenon (Naeiji et al., 2019b, 2019a, 2017, 2016). It should be noted that The *NPT* ensemble was implemented in all directions. To solve the motion equation and obtain the motion trajectory of atoms, the Verlet algorithm was also used (Grubmüller et al., 1991). All simulations were conducted under the prevailing P-T conditions (2 Mpa and 260 K; 3 Mpa and 275 K) to identify

the molecular mechanisms, responsible for the CO_2 crystal growth in the absence or presence of combined additives.

3. Results and discussion

This section deals with analysing the synergistic impacts of additives on CO_2 hydrate growth. However, since the goal of doing simulations was to study the effect of a different set of additives on CO_2 hydrate growth, the main focus was not on the interactions of individual additives with water molecules at the surface. To do so, different parameters such as hydrate growth thickness, potential energy, three-body structural order (F_3), number of hydrogen bonds (H-bonds), mean squared displacement (MSD), radial distribution function (RDF), and the composition of the solution phase was computed. The results of the impacts of mentioned additives in Table 1 on CO_2 hydrate growth at two different thermodynamic conditions are presented in the following sub-sections.

3.1. Hydrate growth thickness

Understanding the transport properties of the dense hydrate phase is pivotal in identifying the controller mechanisms of the hydrate formation and stability. Recent experimental reports on the mass transfer mechanism of gas hydrate formation from water droplets via X-ray computed tomography at the mesoscopic level (300 μm) showed that due to the outward permeation of water through capillary pores in the hydrate shell, the initial diffusion regime is controlled by the transport of water through the shell. However, the first occurrence of hydrate protrusions changes the mode of water transport from diffusion to permeation (Liang et al., 2022). The investigations of components in the system in terms of how they affect each other at smaller scales e.g. nanometres and nanoseconds would also help to detect the behaviours of components at very early

stages of the hydrate formation. In addition, analysing the growth evolution at the molecular level would bridge the gap that exists at scales, the experiment is unable to get so close to. MD framework suggested that the crystallization mechanism of clathrate hydrates can be segmented into three different steps. The formation of blobs is the first step in which dilute solution is in equilibrium with solvent-separated guest molecules. Clathrate cages are then organized by the water so that the solution forms the amorphous clathrate and subsequently, critical nucleus growth can occur. This stage is followed by amorphous maturation in the crystalline phase in which hydrate grows around the nucleus (Jacobson et al., 2010). Since the clathrate nucleation from the solution of gas and water is a stochastic event that needs much time to form, two first steps were skipped, and the growth stage of CO_2 hydrate was explored in this work. Figure 1 (a) shows the snapshots of the simulation box up to 400 ns at 2 MPa and 260 K. To better understand the evolution of the solution phase, the simulation box was divided into five different sections in which "Si (i: 1-4)" represents the water/gas solution beside the initial sI crystal. As the simulation time proceeded, the hydrate growth occurred at the interface of the solution phase. This Figure also shows that up to 150 ns, most of the CO_2 molecules were entrapped in the hydrate cages and the solution gradually changed from a disordered configuration to an ordered solid hydrate during the simulation time; so that the crystal growth was entirely completed as is shown in the final snapshot after 400 ns. With increasing the regularity of guest-host molecular positions, the formed network structurally remained stable. However, the growth kinetics could be changed once additives were included. Figure 1(b) displays the growth evolution of CO_2 hydrate in the presence of mixed metal particles (Cu and Fe) and urea. It can be observed that the existence of additives significantly promoted the rate of crystallization for CO_2 clathrate hydrate. The first snapshot demonstrated that after 25 ns, the S2 and S3 zones were converted to hydrate. Then, the formation of the clathrate

layers was extended and almost all the solution regions were converted to hydrate as the simulation time reached 50 ns. The agglomeration of metal particles in the solution is also evident. The snapshot of the simulation box at 150 ns shows that the position of guest-host molecules was changed slightly but such alterations were toward a better arrangement of water molecules in the clathrate structure.

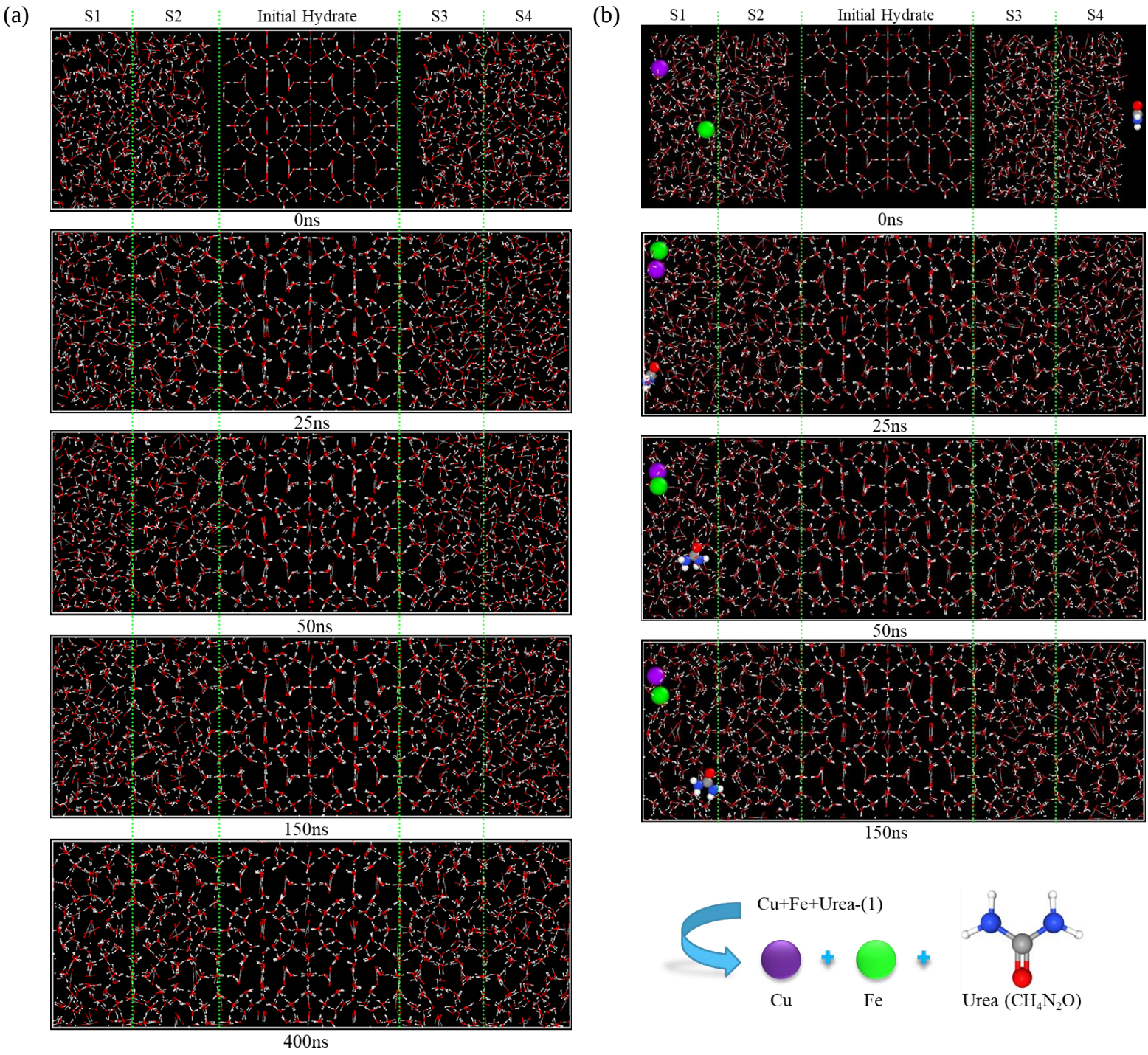

Figure 1: The snapshots of the CO_2 hydrate simulation for (a) pure water, and (b) Cu+Fe+Urea-(1) at 260 K and 2 MPa.

(white atoms: H; red atoms: O; gray atoms: C)

Figure 2 exhibits the thickness of the CO_2 hydrate layer for the first 50 ns of the simulation time. To determine the thickness of the CO_2 hydrate layer, image processing was utilized. By growing the hydrate phase as a function of time, the snapshots were generated every 0.5 ns. The thickness of the hydrate slab from two interfaces was analyzed and finally, the results after 10, 30, 50, 100, and 150 ns of simulation time were reported as indicated in Figure 2. As is shown, the influences of metal particles under different thermodynamic conditions are dissimilar. The addition of combined metal particles to the solution at 260 K seems to be inefficient for the growth rate of the CO_2 hydrate layer. However, the process of hydrate crystallization was positively influenced by the mixture of additives including urea. According to Figure 2 (b), the thickness of CO_2 clathrate above the ice point of water was accelerated when Cu+Ag+Fe metal particles were placed in the solution. Interestingly, the growth rate of the sI slab could even be increased once urea was also included. Although the synergic of additives e.g. mixed metal particles and urea at either below or above water freezing point may positively affect the formation process of CO_2 hydrate, the mixed components in some cases cannot be efficient as either stand-alone utilization of these components or even pure water. Therefore, the following analysis parameters discuss the behaviour of these components during the CO_2 hydrate growth phenomenon.

(a)

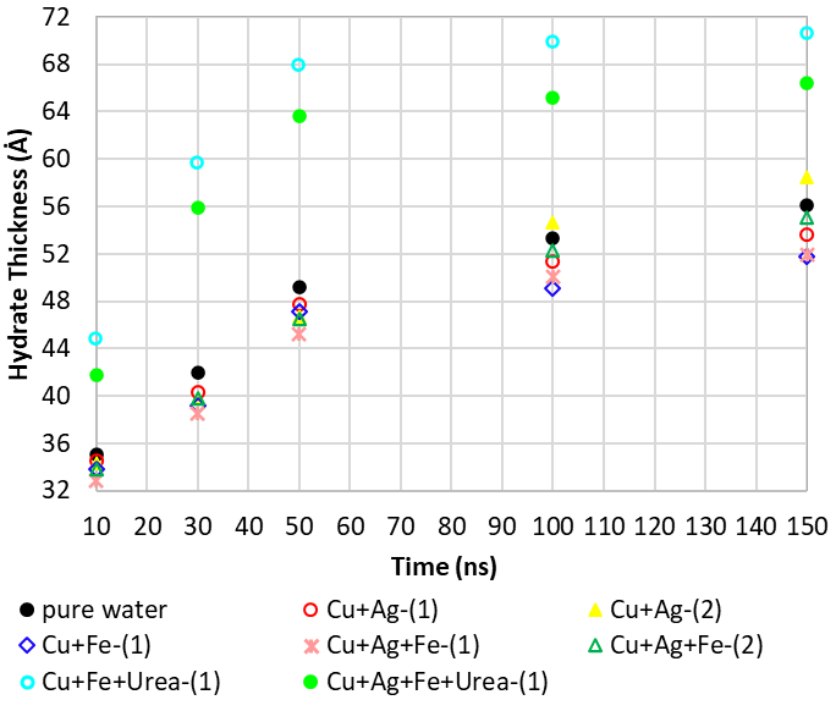

(b)

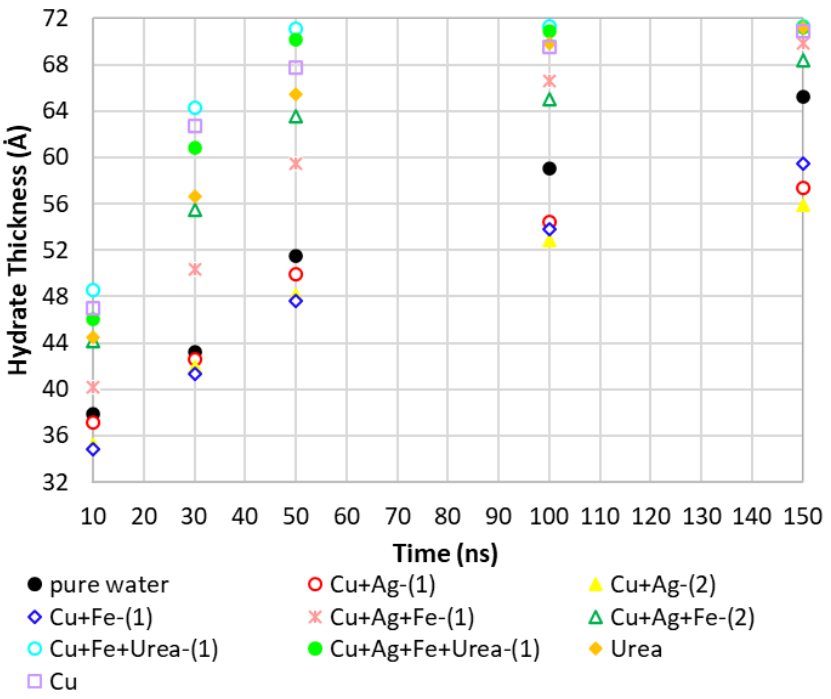

Figure 2: Hydrate thickness (a): at 260 K and 2 MPa; (b) at 275 K and 3 MPa.

3.2. The time variation of potential energy analysis

Analysing the potential energy of the simulated systems can help to reflect the thermodynamic stability and circumstance of gas hydrate at different P-T conditions. The energy for an unstable system is generally prone to abrupt changes but the steady-state creates the situation under which the energy of the system fluctuates around a specific value. The potential energy of the simulated CO_2 hydrates for the cases of either pure water or the presence of combined additives is shown in Figure S1. The downward trend of curves in all systems implies the growth of the initial hydrate slab due to the rearrangements of the solution phase. The more the decline, the higher the growth rate. This Figure shows that the variation of the potential energy of the system in the presence of Cu+Ag, Cu+Fe, and Cu+Ag+Fe-(1) is slightly higher than that of the pure system at 2 MPa and 260 K which indicates that the metal particles at this temperature could not induce the exothermic formation of CO_2 hydrate. Also, the behaviour of Cu+Ag+Fe-(2) in the system is similar to that of pure water. It seems that mixed metal particles under the above-mentioned T-P condition are not only unable to boost the CO_2 crystal growth, but some of which might even slightly inhibit the hydrate formation. However, the mixture including the urea molecule helped to accelerate the decrease of potential energy. This difference is more visible after 50 ns of the simulation time where the fluctuation of Cu+Ag+Urea-(1) reaches the lower potential energy. It can be inferred that with the addition of urea to the primary metal particles, the stability of partially hydrogen-bonded water molecules was maintained, and on the other hand, the amount of mobility and consequently atomic movement in the solution was increased. Also, the amount of interatomic distance was probably increased which might create a space in the atomic space and caused more oscillations of the particles. Since the interaction force between particles is inversely proportional to the distance between particles, it can be expected that the number of atomic interactions and the dependence of the particles on each other was reduced by enhancing oscillations. Once, the P-T

circumstance was altered to 275 K and 3 MPa, some mixed metal particles appeared differently. As Figure S1 (*b*1 and *b*2) present, the addition of Cu+Ag+Fe-(1) to the system decreased the potential energy to lower values, therefore, showing a positive impact. This alteration emerged evidently after 30 ns. However, the presence of Cu metal shows higher performance in comparison with the metal mixtures. This may be because of the regular creation of the active Brownian motion in the solution phase by Cu metal which boosts the rapid transfer of energy. Generally, metal particles due to their high surface are in a state of overactivation so that they may attract each other to form secondary metal clusters if high numbers of those are in the solution phase. In addition, with the higher concentration of metal particles, Cu+Ag+Fe-(2) was somewhat more inducing the reduction rate of potential energy. The synergy of Cu+Ag+Fe-(1) with urea also accelerated the aforementioned reduction. Interestingly, this enhancement in the absence of Ag was even higher. Since the behaviour of the system including either Cu+Ag or Cu+Fe was quite dissimilar, it can be concluded that the synergistic of metal particles cannot be always successful. Moreover, the thermodynamic condition can also be one of the main contributors. Indeed, the T-P condition of the system would be determinative in the performance of additives. By comparing the CO_2 hydrate growth at below and above water freezing points, it can be deduced that the growth process in the presence of metal particles is more prone to change than the systems with urea once the thermodynamic condition was altered from 260 K to 275 K. It can also be assumed that metal particles and urea might intrinsically affect heat and mass transfer coefficients of the solution phase respectively. Since the collision of metal particles with water molecules can accelerate the relative motion of the solution phase, a such local disturbance may improve the energy transfer between the original molecules of both CO_2 and water in the system which would contribute to creating the effective formation of hydrogen bonds between water molecules.

3.3. Hydrogen bonding of CO_2 crystal growth

The number of hydrogen bonds (H-bonds) has a close relationship with the ordered crystal of clathrate hydrate. The more conversion of disordered liquid molecules to arranged shapes gives a higher number of H-bonds. The tetrahedral cages are gradually formed by the H-bond connections across water molecules. The time variation of the number of H-bonds during the CO_2 hydrate formation in contact with different additives in the solution is shown in Figure S2. For both thermodynamic simulation conditions in this figure, the number of H-bonds from the initial time to 150 ns has been increased from 616 to over 1500 which indicates that the hydrate crystal was steadily growing. The trend of H-bonds reached a plateau value as the process of crystal formation came to the end. As is evident in Figure S2 (*a*1 and *a*2), the highest number of H-bonds was obtained for the system including Cu+Fe+Urea-(1) which properly promoted the CO_2 hydrate formation. The average and maximum number of H-bonds for pure water were 1511 and 1603 while that for Cu+Fe+Urea-(1) were 1547 and 1640 respectively. A higher number of H-bonds for the latter system may indicate that an orderly arrangement of the water molecules in the clathrate was upgraded. This might be due to the surface of the urea molecule which creates several hydrogen bonds with two or three adjacent cages of water molecules. The oxygen atom of urea prefers to align slightly towards the hydrate phase. It was found that the oxygen atom in urea is aligned toward the hexagonal face of the large cage. The distance between this atom in urea and cage water was ~ 2.5 Å which indicates the close interactions of this molecule with the hydrate cage. Since urea molecule can help to stabilize the cages at the hydrate surface, the more regular water molecules in the network can be formed. In addition, the undesirable local interactions of Cu and Fe metal particles may be inappreciable due to the lower operating temperature (260 K). However, in the presence of Ag metal, the disturbance motions of Ag compensate the more regular

algorithm of water molecules in the clathrate structure of CO_2 hydrate. Hence, the inclusion of Ag in this mixture (Cu+Ag+Fe+Urea-(1)) slightly slowed down the hydrate growth. Based on Figure S2 (*a*1 and *a*2), the promotion effect of the Cu+Fe binary and the Cu+Ag+Fe ternary mixtures in comparison with the pure water system was no longer significant. Also, the addition of Cu+Ag at two different concentrations slightly acted as an inhibitor which resulted in a lower number of H-bonds. However, according to Figure S2 (*b*1 and *b*2), the behaviour of combined additives at 3 MPa and 275 K are somewhat different. Although the presence of pure Cu and urea molecule were quite efficient in increasing the number of H-bonds, the combined Cu+Ag+Fe, Cu+Ag+Fe-Urea-(1), and Cu+Fe-Urea-(1) by providing plenty of nucleation sites might elevate the effectiveness of the surface area in the solution phase. In contrast, Cu+Ag and Cu+Fe decreased the amount of H-bonds. It should be highlighted that during the process of CO_2 hydrate formation, the heat released raises the temperature of the system and subsequently weakens the effective driving force. So that, since metal particles mostly possess high thermal conductivity, they can evenly distribute the generated heat at the local liquid-solid interface. The heat and mass transfer of the solution can also be increased by enhancing the electrical conductivity but the optimal state may give a higher performance. The order of electrical conductivity for the mixed metal atoms from low to high are Cu+Fe, Cu+Ag+Fe, and Cu+Ag respectively (Zuo et al., 2017). Therefore, Cu+Ag+Fe in comparison with two other coupled metal atoms might be closer to the optimum condition. This is indicated that the mixed metal particles have various impacts on the enhancement of the kinetics of the hydrate growth process. In addition, the atomic mass may contribute to the formation of local perturbations. Since the Ag atomic mass (108) is considerably different from Cu (64) and Fe (56), the Ag atom has a smaller motion speed and ability to promote local convection rather than either Cu or Fe. Based on the results of the simulation, it can be assumed that there is a

correspondence relating the potential energy with the number of H-bonds. The higher reduction of potential energy at the final stage of the simulations may give a higher number of H-bonds. Table 2 indicates some information about the correspondence of these two analysis parameters. Therefore, by plotting the evolution of potential energy versus the number of H-bonds, it can be considered that the higher slope of simulated systems than that of pure water may show the promotion impacts of the included additives.

Table 2: Correspondence relating the potential energy and the number of H-bonds at 3 MPa and 275 K.

	pure water		**Cu+Ag-(1)**		**Cu+Ag-(2)**		**Cu+Fe-(1)**		**Cu+Ag+Fe-(1)**	
	PE	HB	PE	HB	PE	HB	PE	HB	PE	HB
Min.	-16894	1286	-16862	1306	-16831	1293	-16943	1288	-17007	1293
Avg.	-16676	1481	-16670	1466	-16642	1450	-16638	1460	-16824	1504
Max.	-15620	1574	-15555	1542	-15596	1541	-15712	1573	-15420	1614
Y=*a*X+*b*	*a*: -0.27, *b*: -3013		*a*: -0.26, *b*: -2817		*a*: -0.25, *b*: -2708		*a*: -.26, *b*: -2920		*a*: -0.28, *b*: -3321	
	Cu+Ag+Fe-(2)		**Cu+Fe+Urea-(1)**		**Cu+Ag+Fe+Urea-(1)**		**Urea-(1)**		**Cu**	
	PE	HB	PE	HB	PE	HB	PE	HB	PE	HB
Min.	-17034	1306	-17049	1329	-17038	1284	-16994	1315	-17017	1288
Avg.	-16837	1486	-16867	1519	-16840	1514	-16803	1516	-16853	1515
Max.	-15443	1576	-15229	1609	-15261	1592	-15195	1602	-15320	1597
Y=*a*X+*b*	*a*: -0.28, *b*: -3197		*a*: -0.30, *b*: -3530		*a*: -0.29, *b*: -3461		*a*: -0.29, *b*: -3385		*a*: -0.30, *b*: -3484	

Note: the "PE" and "HB" represent the potential energy and the number of hydrogen bonds respectively; PE in the linear equation (as an X) gives the number of HB.

3.4. The structural order parameter of clathrate hydrate

Computing the order parameter F_3 for water molecules in a specific region or total simulation box as a function of time can help to quantify the CO_2 hydrate growth along the Z-axis. This parameter

displays the deviation of the oxygen positions in the water triplets from the tetrahedral arrangement in the clathrate. The F_3 parameter is defined as the below equation (Bagherzadeh et al., 2012):

$$F_3 = \frac{1}{n}\sum_i^n \left(\left|cos\theta_{jik}\right| cos\theta_{jik} + cos^2(104.52°)\right)^2 \quad (1)$$

Where *j*, *i*, and *k* represent three oxygen atoms of water molecules to take into account a tetrahedral arrangement of water molecules that are close together, and atom *i* is located in the center of a spherical shell of 3.5 Å including atoms *j* and *k*. The value (104.52) in the equation is the H-O-H angle of water molecules from the TIP4P/ice model. Once the solution phase was ordered, the F_3 order parameter converges to nearly zero whereas the F_3 for the liquid phase is around 0.1. Figure S3 reveals the total F_3 parameter of the simulation box at two investigated operating conditions. As is evident, values of F_3 as a function of time decreased from 0.05 to less than 0.02 by the end of the simulations. This implies that the hydrate formation extends along the simulation box. There is a similarity between the results obtained from the F_3 values and those from the potential energy evaluated in the previous section. At 260 K, the decline of the F_3 curve for the systems including Cu+Ag and Cu+Ag+Fe was not substantial. Therefore, the slope of the F_3 is less than the absence of metal particles. Also, the impression of systems with urea is more apparent when 50 ns of simulation time is passed. Interestingly, the F_3 after the aforesaid time was reduced to below 0.015 for the case of Cu+Fe+urea while by adding Ag to this mixture, the performance of the additives was lowered and the F_3 value fluctuates between the former case and the system with pure water. This may indicate that Ag reduces the promotion capability of Cu+Fe+urea-(1) by creating uncoordinated movements. Also, the F_3 amount for the combined additives which converged to less than 0.015 indicates that the formation of the solid phase is more regular and rapid than in other systems. However, the behaviour of additives at 275 K is not similar to those under the water ice point. Although Cu+Ag and Cu+Fe are unable to desirably reduce the F_3 order parameter, the

ternary of Cu+Ag+Fe with different concentrations possesses a positive impression on decreasing the F_3 parameter. For the lower and higher concentrations of ternary metal additives, the F_3 declined at about 60 ns and 40 ns respectively. This may reveal that a greater concentration was closer to the optimized condition. While the F_3 drop in the existence of synergistic Cu+Ag+Fe+urea-(1) occurred at 30 ns.

Although the results of the utilization of pure urea are substantial, the Cu+Fe+urea-(1) led the decline time of F_3 to around 20 ns which represents the most superior improvement of this combination on the extension of clathrate growth. It should be noted that urea has no particular affinity to the hydrate-solution interface but prefers to stay near the liquid-gas interface. Urea molecule is neither entrapped in the clathrate nor blocks the hydrate growth. However, urea may firstly be entrapped in partially formed cavities and then replaced with guest CO_2 molecules to complete the cages as it was certified elsewhere (Wang et al., 2021). It is also essential to consider that in the case of binding additives to the hydrate surface over the characteristic time of clathrate formation, the process of hydrate growth can be hindered. Probably, the residence time of urea near the solid surface is less than the characteristic time of the crystal growth. Therefore, hydrate growth was not blocked by the urea molecule.

To further investigations about the effects of additives on the solution segments neighbour the sI slab, analysing the section-wise F_3 calculations would be advantageous. Figure 3 exhibits the F_3 parameter in the solution around the hydrate slab for pure water, Cu+Ag+Fe-(2) and Cu+Ag+Fe+Urea-(1) at two different T-P conditions. It seems that the reduction of F_3 for all systems irrespective of the operating condition is firstly started from the solution layers just beside the hydrate slab (S2 and S3) and then extended toward the end sides of the Z-axis of the simulation box (S1 and S4). This may be evidence of the inherent growth mechanism of crystallization in

contact with the hydrate phase. Consistent with preceding expressions, the decrease of the F_3 parameter during simulation time at 260 K for Cu+Ag+Fe and Cu+Ag+Fe+Urea are slower and quicker than pure water respectively. However, as Figures 3 (d) and (f) show, both combinations possess the promotion behaviour in comparison with their absence which is displayed in case (b). By comparing Figures 3 (a), (c), and (e), it can be observed that although the synergic of Cu+Ag+Fe improves the heat transfer flow, the Brownian motion may act as a disturbance of partially formed cavities near the initial slab. However, the inclusion of urea by facilitating the formation of half cages restrains the disordering motions of water molecules. Therefore, the growth in Figure 3 (e) after passing 60 ns can be completed while it did not occur for cases (a) and (c). Figure 3 (b) also kinetically exhibits that, the process of crystallization for pure water at 275 K was increased which signifies that the lower subcooling may not always give a faster rate of hydrate crystallization. Similar behaviour can also be seen in cases (d) and (f). In contrast with case (c), the presence of metal particles acted as a vigorous promoter which reduced the drop time of F_3 value from over 100 ns in case (b) to slightly above 40 ns in case (d). This time in case (f) was also shortened to 30 ns once urea was included. Interestingly, the presence of urea regardless of thermodynamic condition reduces the fluctuation of the F_3 parameter in all fourth regions of the solutions. This implies that the urea molecule by alleviating the vibrations of ordered water molecules due to inducing the better distribution of CO_2 molecules between water molecules may help to extend and then maintain the stability of formed hydrate.

(a)

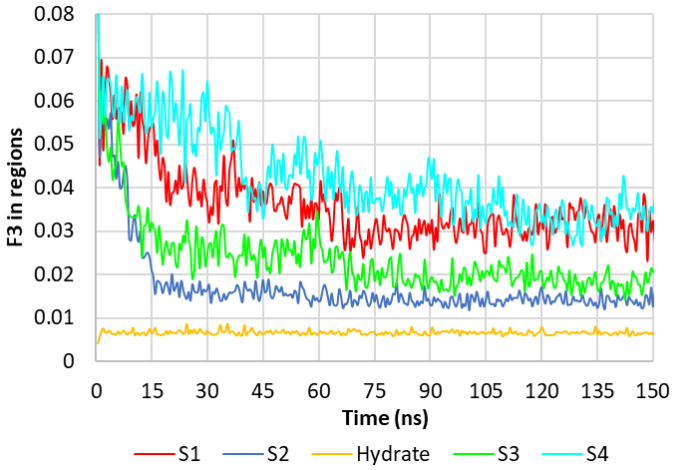
F3 in regions
0.08
0.07
0.06
0.05
0.04
0.03
0.02
0.01
0
0 15 30 45 60 75 90 105 120 135 150
Time (ns)
S1 S2 Hydrate S3 S4

(b)

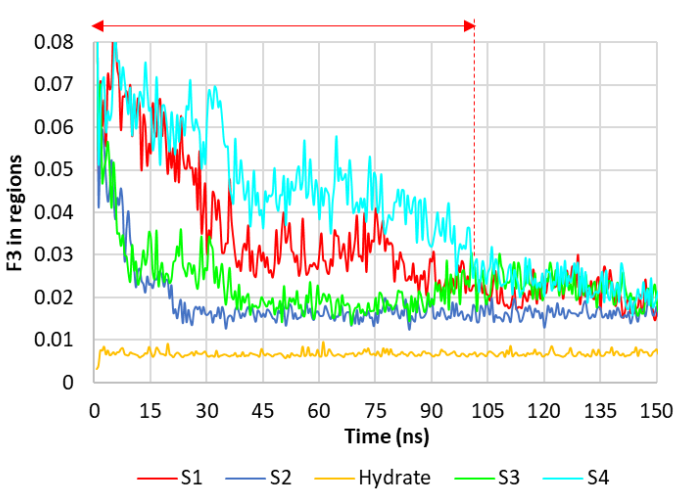
F3 in regions
0.08
0.07
0.06
0.05
0.04
0.03
0.02
0.01
0
0 15 30 45 60 75 90 105 120 135 150
Time (ns)
S1 S2 Hydrate S3 S4

(c)

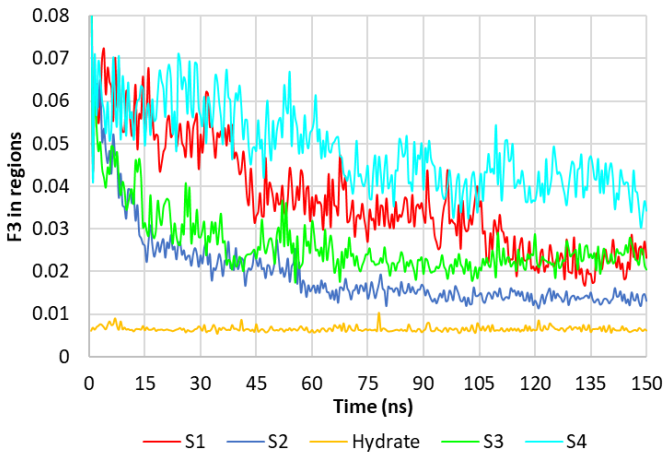
F3 in regions
0.08
0.07
0.06
0.05
0.04
0.03
0.02
0.01
0
0 15 30 45 60 75 90 105 120 135 150
Time (ns)
S1 S2 Hydrate S3 S4

(d)

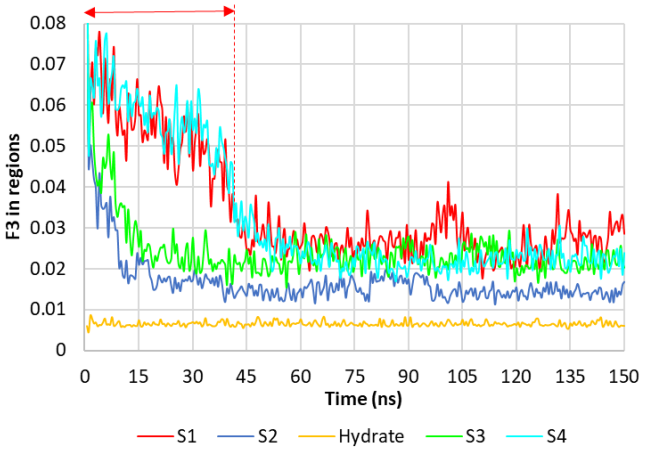
F3 in regions
0.08
0.07
0.06
0.05
0.04
0.03
0.02
0.01
0
0 15 30 45 60 75 90 105 120 135 150
Time (ns)
S1 S2 Hydrate S3 S4

(e)

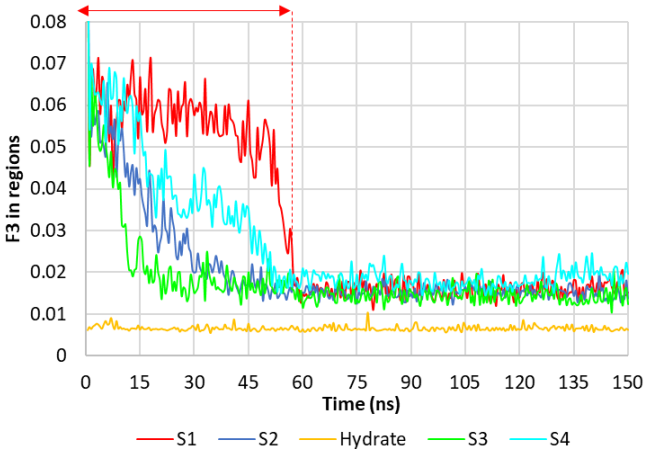
F3 in regions
0.08
0.07
0.06
0.05
0.04
0.03
0.02
0.01
0
0 15 30 45 60 75 90 105 120 135 150
Time (ns)
S1 S2 Hydrate S3 S4

(f)

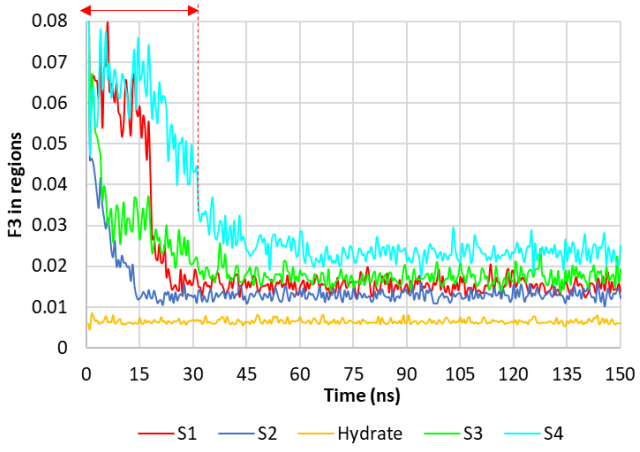
F3 in regions
0.08
0.07
0.06
0.05
0.04
0.03
0.02
0.01
0
0 15 30 45 60 75 90 105 120 135 150
Time (ns)
S1 S2 Hydrate S3 S4

Figure 3: F_3 order parameter of CO_2 hydrate growth in the different slabs of the simulation box along the *z*-direction for (a) and (b), pure water; (c) and (d), Cu+Ag+Fe-(2); and (e) and (f), Cu+Ag+Fe+Urea-(1). Cases (a), (c), and (e) were performed at 260 K and 2 MPa while (b), (d), and (f) were carried out at 275 K and 3 MPa.

3.5. Diffusion behaviour of the particles

Atoms in particle diffusion systems tend to diffuse into space. Therefore, the mean square displacement (MSD) of atoms shows their diffusion and mobility in a system. Since particles cannot freely diffuse through the solid state, the MSD of components in liquid and gas phases is significantly higher than in the solid (hydrate) phase. To distinguish the phases, this parameter is applied which can be expressed by the following equation (Naeiji et al., 2019a):

$$MSD = \frac{1}{N}\sum_{i=1}^{N}\left|R^i(t) - R^i(0)\right|^2 \quad (2)$$

Where R is the position of atom i at times t and 0; N represents the total number of atoms. MSD of all molecules in the simulation box for all simulated systems at two different thermodynamic conditions is plotted in Figure S4. As is shown at 260 K, the MSD curve of systems with urea after a specific simulation time reaches a plateau whereas the systems in the presence of metal particles are still unstable. This indicates that the solution for the systems with urea almost converted to the solid state, while the growth process for the systems with metal particles was not fulfilled. Consistent with the results of the previous sections, the behaviour of Cu+Ag+Fe metal particles at 275 K is quite different and their MSDs after about 40-50 ns approached to the constant value. This is also valid for the solution including pure Cu and urea which occurred at around 30 ns whereas MSD for the combined Cu+Fe+urea-(1) stabilized at 20 ns. Due to the somewhat inhibitor effects of binary combined metal particles, the higher mobility in the system resulted in increasing

MSDs above 50 ns while most of the solution phase for the other systems converted into the clathrate hydrate so that their MSDs converged to almost a flat trend.

Analysing the MSD of water molecules can also help to understand how additives change the water arrangement in the solution phase. Figure 4 manifests the MSD of water molecules in four distinct areas of the solution besides the sI hydrate slab. The mixed additives at 275 K shown in Figure 4 (a) acted as an accelerator of hydrate formation while the combinations presented in Figure 4 (b) are found to somewhat prevent the hydrate growth. The smooth slopes of MSD in Figure 4 (a) reflect that the additives successfully impressed host molecules and locate themselves in guest-host positions of sI clathrate. Moreover, the ordered arrangement of water molecules began firstly in the S2 and S3 segments of the solution (at nearly 20 ns) and subsequently occurred in S1 and S4 at over 30 ns. Additionally, the MSD approach of systems with additives in all fourth regions was under that of pure water. As Figure 4 (b) shows, the Cu+Ag and Cu+Fe also inclined the trend of water's MSD when they were included in the solution. This behaviour is also observed in all segments as simulation time passed. It seems that in these systems, the movements caused by the existence of metal particles disturb the local arrangement of water molecules.

(a)

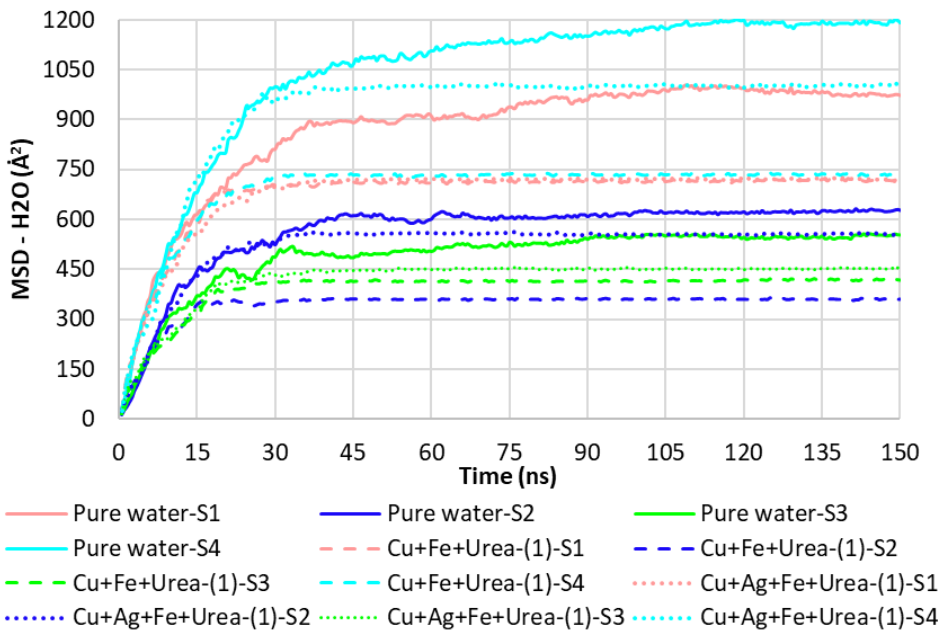

(b)

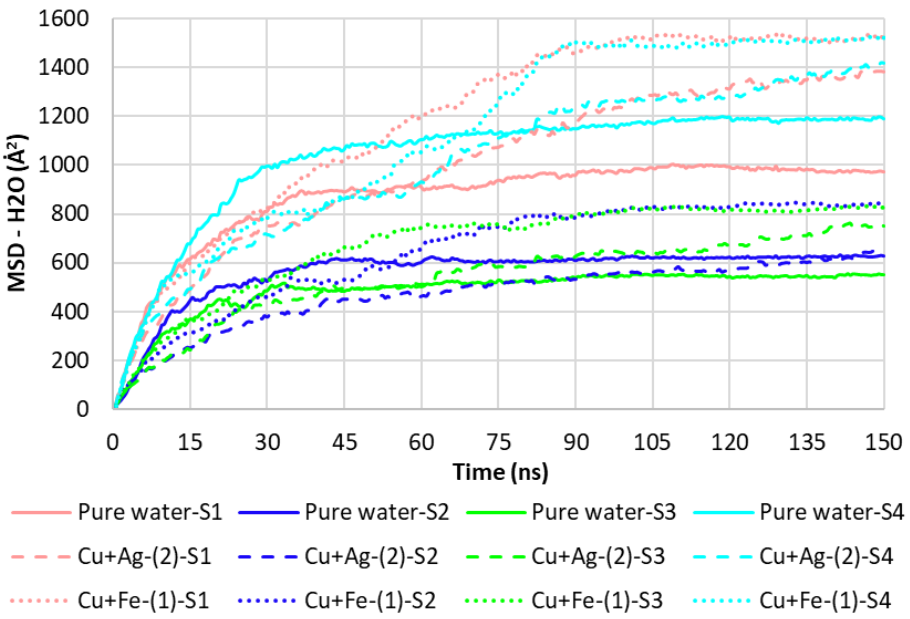

Figure 4: MSD of water molecules in different regions of the simulation box at 275 K and 3 MPa. (a): a combination of metal particles and urea; (b) a binary mixture of metal particles (The regions are defined in Figure 1)

3.6. Water molecules in the hydrate structure

To determine the degree of ordered molecules in the hydrate structure and describe the configuration of the formed clathrate, the radial distribution function (RDF) was also investigated. The following equation represents the degree of ordered molecules in the system, where the probability of particle β distribution around a given particle α is counted. Vs, Nα, and Nβ denote the volume of the simulation box, and the number of particles α and β respectively.

$$g_{\alpha\beta} = \frac{V_s}{N_\alpha N_\beta}\left[\sum_{i=1}^{N_\alpha} \frac{N_{i\beta}(r)}{4\pi r^2 \Delta r}\right] \quad (3)$$

The RDF between oxygen atoms of water molecules in the system is displayed in Figure S5. As is evident, the first significant peak occurred at 2.75 Å which relates to the adjacent H_2O molecule. The second shorter peak at 4.5 Å reflects the tetrahedral nature of the water cage. The lowest peak appeared at 6.45 Å which is the distance between oxygen atoms of H_2O molecules spaced apart in the hydrate cage. It should be pointed out that the calculated RDF in this work is qualitatively in agreement with the reported values in the literature (Liu et al., 2021; Mahmoodi et al., 2021). By comparing the RDF of water molecules at 260 K and 275 K, it can be concluded that the peak height became slightly greater as well as narrower once the temperature was lowered. This may indicate the more ordered water molecules and higher number of H-bonds in the clathrate. Besides, the similar Peaks of systems with or without additives implies that these components cannot significantly change the local arrangement of water molecules. As Figure S5 (*a*3) exhibits, the height of the first peak for pure water is located above the systems with metal particles but under the systems with urea. The binary mixture of metal particles in Figure S5 (*b*3) also seems to be ineffective. In addition, the first RDF peak of H_2O atoms for the system with the presence of Cu+Ag+Fe-(1) remained unchanged when urea was included. There is a striking resemblance between the highest peak of Cu+Fe+urea-(1) and Cu+Ag+Fe-(2), however, both of which were

established over the earlier mentioned solution systems. Therefore, it can be deduced that the promotion of a ternary mixture of Cu, Ag, and Fe metal particles at 275 K in ordered water molecules of clathrate hydrate is more appreciable than either utilization of single urea or pure Cu metal particles.

3.7. Guest and host distribution in the solution phase

Through MD simulations, it was reported that when urea is present, the relative concentration of CO_2 in the water phase is near unity and the CO_2 concentration gradient is markedly lowered. It was also estimated that urea increases the mass transfer coefficient of CO_2 by nearly 6 times, therefore, this component enhances the mass transport and the formation rate of the system (Wang et al., 2021). It seems that the self-diffusivity of water molecules and CO_2 solubility may be boosted when urea is in the system. Presumably, urea catalyses the ring structure of hydrate formation but does not block the crystal growth process. Therefore, the surface of urea might help water molecules to arrange themselves in form of pentagonal and hexagonal rings. The oxygen and nitrogen atoms in the molecular structure of urea, by dragging the H-bonded water molecule, serve as a hydrogen acceptor. Therefore, the oxygen atoms tend to align towards the hydrate phase. Figure 5 compares the regional distribution of CO_2 and H_2O molecules for pure water and Cu+Fe+Urea-(1) systems at 3 MPa and 275 K. As is shown, there is a pleasant convergence in the oscillation of guest and host molecules for the system with urea. According to the stoichiometric of CO_2 sI clathrate hydrate, the number of CO_2 and water in each segment of the solution need to be equal to 32 and 184 molecules respectively. Since the growth starts to expand from the boundaries of the solution phase with the sI hydrate slab, the neighbouring solution sides of the hydrate are more prone to form the clathrate structure. Therefore, they converge to the stoichiometric values more quickly than two further sections. These regions in the existence of

Cu+Fe+Urea-(1) are almost approaching the stoichiometric amounts of CO_2 sI hydrate after passing the first 30 ns. In addition, the aforementioned synergic promoters by increasing the diffusivity of guest and host molecules most likely moderate the irregular distribution of the solution phase.

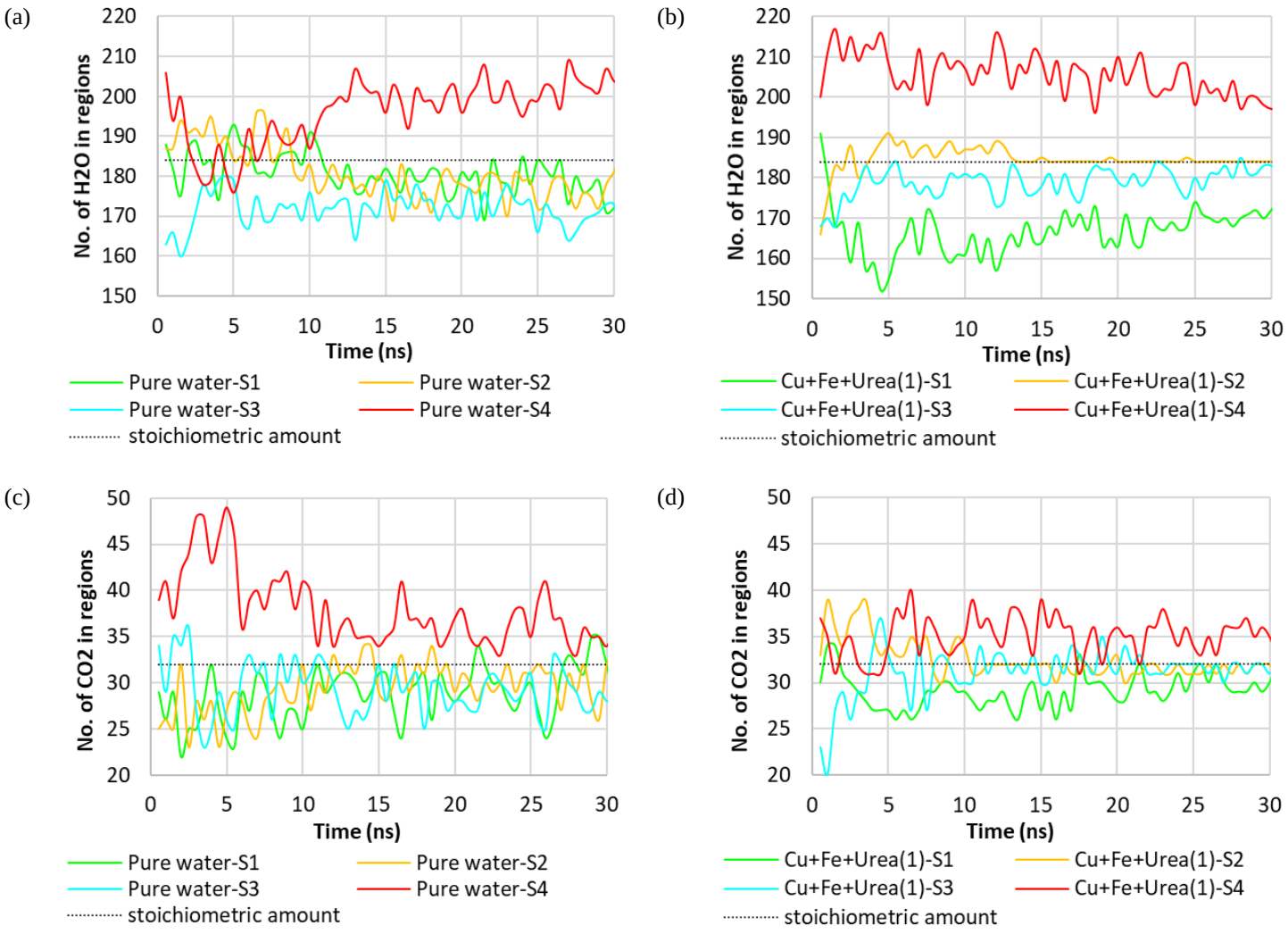

Figure 5: Comparison of the number of water and CO_2 molecules between the systems including (a) and (c) pure water; (b) and (d) Cu+Fe+Urea-(1), at 275 K and 3 MPa.

1. Conclusion

Since the synergistic promoters may not always be favourable for the formation of gas hydrates, the main contributors to such combinations need to be investigated to find the optimized circumstances, particularly in terms of studying the types of combined additives, their concentrations in the mixture, and operating conditions. The simulation results of this work demonstrated that the synergic mixtures of metal particles (Cu, Ag, Fe) and urea can accelerate the process of CO_2 hydrate growth by increasing the heat and mass transport of the solution at the solid-liquid interface respectively. The formation rate was even maximized when the aforementioned mixed additives without Ag were used. The addition of mixed metal particles and urea can positively induce host and guest molecules in the solution regions and help them be more properly organized. Interestingly, the mentioned synergistic promoters can efficiently work below and above the water ice point. However, the results of the solution systems including just metal particles showed that their behaviour mostly varies depending on the temperature and pressure of the system. The inclusion of Cu+Ag+Fe with two different concentrations in the solution phase enhanced water molecules to locate themselves in the form of hydrogen-bonded crystalline structure above the water solidification point. The addition of Cu+Ag and Cu+Fe to the system either below or above the water freezing point reduced the orderly movement of water molecules by increasing the potential energy and Brownian motion in the system. The growth kinetics of CO_2 hydrate in the presence of a single urea molecule and pure Cu metal particles are also close to the cases when their combinations were used. However, the higher arrangement of water molecules in the network of the clathrate hydrate for the mixed metal particles and urea was observed. Furthermore, when higher subcooling (260 K) was imposed, lower CO_2 hydrate growth was observed. This implies that the higher subcooling does not always result in quicker crystallization.

Also, the crystallization in all simulated cases irrespective of operating conditions and additive types was started from the interface and then expanded in neighbouring layers of the solution.

Conflict of interest

The authors declare no conflicts of interest.

Acknowledgments

The first author would like to thank Curtin University Malaysia for providing Curtin Malaysia Postgraduate Scholarship (CMPRS), financial support for this project, and Pawsey Supercomputing Centre for facilitating the project with supercomputers. We are also grateful to Dr. Saman Alavi from the University of Ottawa for his valuable feedback on this work.

Nomenclature

MD	Molecular Dynamics	ns	nano-second
Ag	Silver	ps	pico-second
Fe	Iron		*Greek letters*
Cu	Cupper	a	Atom a
PE	Potential Energy	b	Atom b
MSD	Mean Squared Displacement	ε	Cross LJ parameters
F_3	Three-body Structural order	σ	Cross LJ parameter
RDF	Radial Distribution Function	θ	Angle
g_{ab}	RDF between atoms a and b		*Subscripts*
P	Pressure	i	Atom i
T	Temperature	j	Atom j

K	Kelvin	*k*	Atom *k*
MPa	Mega Pascal	x	x direction
Å	Angstrom	y	y direction
HB	Hydrogen bonds	z	z direction

References

Abascal, J.L.F., Sanz, E., García Fernández, R., Vega, C., 2005. A potential model for the study of ices and amorphous water: TIP4P/Ice. J. Chem. Phys. 122, 234511. https://doi.org/10.1063/1.1931662

Adibi, N., Mohammadi, M., Ehsani, M.R., Khanmohammadian, E., 2020. Experimental investigation of using combined CH4/CO2 replacement and thermal stimulation methods for methane production from gas hydrate in the presence of SiO2 and ZnO nanoparticles. J. Nat. Gas Sci. Eng. 103690. https://doi.org/10.1016/j.jngse.2020.103690

Ayittey, F.K., Obek, C.A., Saptoro, A., Perumal, K., Wong, M.K., 2020a. Process modifications for a hot potassium carbonate-based CO2 capture system: a comparative study. Greenh. Gases Sci. Technol. 10, 130–146. https://doi.org/10.1002/ghg.1953

Ayittey, F.K., Saptoro, A., Kumar, P., Wong, M.K., 2021. Energy-saving process configurations for monoethanolamine-based CO2 capture system. Asia-Pacific J. Chem. Eng. 16, 1–15. https://doi.org/10.1002/apj.2576

Ayittey, F.K., Saptoro, A., Kumar, P., Wong, M.K., 2020b. Parametric study and optimisation of hot K 2 CO 3 - based post-combustion CO 2 capture from a coal-fired power plant. Greenh. Gases Sci. Technol. 10, 631–642. https://doi.org/10.1002/ghg.1983

Babu, P., Nambiar, A., He, T., Karimi, I.A., Lee, J.D., Englezos, P., Linga, P., 2018. A review of clathrate hydrate Bbased desalination to strengthen energy–water nexus. ACS Sustain. Chem. Eng. 6, 8093–8107. https://doi.org/10.1021/acssuschemeng.8b01616

Bagherzadeh, S.A., Englezos, P., Alavi, S., Ripmeester, J.A., 2012. Molecular simulation of non-equilibrium

methane hydrate decomposition process. J. Chem. Thermodyn. 44, 13–19. https://doi.org/10.1016/j.jct.2011.08.021

Cann, D., Font-Palma, C., Willson, P., 2021. Experimental analysis of CO2 frost front behaviour in moving packed beds for cryogenic CO2 capture. Int. J. Greenh. Gas Control 107, 103291. https://doi.org/10.1016/j.ijggc.2021.103291

Chen, C.H. Ho, Y.., 2017. Measurement of Thermodynamics and Kinetics of Carbon Dioxide Hydrate in the Presence of Urea and 1,3-Cyclohexanebis (methylamine). National Taiwan University.

Dhoke, C., Zaabout, A., Cloete, S., Amini, S., 2021. Review on Reactor Configurations for Adsorption-Based CO 2 Capture. Ind. Eng. Chem. Res. 60, 3779–3798. https://doi.org/10.1021/acs.iecr.0c04547

Eggimann, B.L., Sunnarborg, A.J., Stern, H.D., Bliss, A.P., Siepmann, J.I., 2014. An online parameter and property database for the TraPPE force field. Mol. Simul. 40, 101–105. https://doi.org/10.1080/08927022.2013.842994

Elwell, L C; Grant, W.S., 2006. Technology options for capturing CO2. Power (New York) 149.

Firoozabadi, S.R., Bonyadi, M., Lashanizadegan, A., 2018. Experimental investigation of Fe3O4 nanoparticles effect on the carbon dioxide hydrate formation in the presence of magnetic field. J. Nat. Gas Sci. Eng. 59, 374–386. https://doi.org/10.1016/j.jngse.2018.09.013

Frenkel, D., Smit, B., 2002. Long-Range Interactions, in: Understanding Molecular Simulation. Elsevier, pp. 291–320. https://doi.org/10.1016/B978-012267351-1/50014-6

Gambelli, A.M., Presciutti, A., Rossi, F., 2021. Review on the characteristics and advantages related to the use of flue-gas as CO2/N2 mixture for gas hydrate production. Fluid Phase Equilib. 541, 113077. https://doi.org/10.1016/j.fluid.2021.113077

Gong, Y., Mendgaziev, R.I., Hu, W., Li, Y., Li, Z., Stoporev, A.S., Manakov, A.Y., Vinokurov, V.A., Li, T., Semenov, A.P., 2022. Urea as a green thermodynamic inhibitor of sII gas hydrates. Chem. Eng. J. 429, 132386. https://doi.org/10.1016/j.cej.2021.132386

Grubmüller, H., Heller, H., Windemuth, A., Schulten, K., 1991. Generalized Verlet Algorithm for Efficient Molecular Dynamics Simulations with Long-range Interactions. Mol. Simul. 6, 121–142.

https://doi.org/10.1080/08927029108022142

Hafizi, A., Rajabzadeh, M., Mokari, M.H., Khalifeh, R., 2021. Synthesis, property analysis and absorption efficiency of newly prepared tricationic ionic liquids for CO2 capture. J. Mol. Liq. 324, 115108. https://doi.org/10.1016/j.molliq.2020.115108

Hockney, R.., Eastwood, J.., 2021. Computer Simulation Using Particles. CRC Press. https://doi.org/10.1201/9780367806934

Idrissi, A., Gerard, M., Damay, P., Kiselev, M., Puhovsky, Y., Cinar, E., Lagant, P., Vergoten, G., 2010. The Effect of Urea on the Structure of Water: A Molecular Dynamics Simulation. J. Phys. Chem. B 114, 4731–4738. https://doi.org/10.1021/jp911939y

Jacobson, L.C., Hujo, W., Molinero, V., 2010. Nucleation pathways of clathrate hydrates: Effect of guest size and solubility. J. Phys. Chem. B 114, 13796–13807. https://doi.org/10.1021/jp107269q

Jiang, W., Wu, F., Gao, G., Li, X., Zhang, L., Luo, C., 2021. Absorption performance and reaction mechanism study on a novel anhydrous phase change absorbent for CO2 capture. Chem. Eng. J. 420, 129897. https://doi.org/10.1016/j.cej.2021.129897

Jokar, S.M., Wood, D.A., Sinehbaghizadeh, S., Parvasi, P., Javanmardi, J., 2021. Transformation of associated natural gas into valuable products to avoid gas wastage in the form of flaring. J. Nat. Gas Sci. Eng. 104078. https://doi.org/10.1016/j.jngse.2021.104078

Kallies, B., 2002. Coupling of solvent and solute dynamics—molecular dynamics simulations of aqueous urea solutions with different intramolecular potentials. Phys. Chem. Chem. Phys. 4, 86–95. https://doi.org/10.1039/b105836n

Liang, H., Guan, D., Shi, K., Yang, L., Zhang, L., Zhao, J., Song, Y., 2022. Characterizing Mass-Transfer mechanism during gas hydrate formation from water droplets. Chem. Eng. J. 428, 132626. https://doi.org/10.1016/j.cej.2021.132626

Lim, L.H. V, Lloren, A.V., Lamorena, R.B., 2014. The effect of urea in the nucleation process of CO2 clathrate hydrates. J. Mol. Liq. 194, 245–250. https://doi.org/10.1016/j.molliq.2014.03.003

Liu, N., Zhu, H., Zhou, J., Yang, L., Liu, D., 2021. Molecular dynamics simulations on formation of CO2 hydrate in the presence of metal particles. J. Mol. Liq. 331, 115793. https://doi.org/10.1016/j.molliq.2021.115793

Liu, Y., Liao, X., Shi, C., Ling, Z., Jiang, L., 2020. Promoting and inhibitory effects of hydrophilic/hydrophobic modified aluminum oxide nanoparticles on carbon dioxide hydrate formation. Energies 13, 5380. https://doi.org/10.3390/en13205380

Machida, H., Hashiride, R., Niinomi, R., Yanase, K., Hirayama, M., Umeda, Y., Norinaga, K., 2021. An Alternative CO 2 Capture with a Pressure Swing Amine Process Driven by Cryogenic Pumping with the Unused Cold Energy of Liquefied Natural Gas. ACS Sustain. Chem. Eng. 9, 15908–15914. https://doi.org/10.1021/acssuschemeng.1c05892

Maddah, Mitra, Maddah, Mina, Peyvandi, K., 2018. Molecular dynamics simulation of methane hydrate formation in presence and absence of amino acid inhibitors. J. Mol. Liq. 269, 721–732. https://doi.org/10.1016/j.molliq.2018.08.108

Mahmoodi, M.H., Manteghian, M., Naeiji, P., 2021. Study the effect of Ag nanoparticles on the kinetics of CO2 hydrate growth by molecular dynamics simulation. J. Mol. Liq. 343, 117668. https://doi.org/10.1016/j.molliq.2021.117668

Míguez, J.M., Conde, M.M., Torré, J., Blas, F.J., Piñeiro, M.M., Vega, C., 2015. Molecular dynamics simulation of CO2 hydrates : Prediction of three phase coexistence line Molecular dynamics simulation of CO 2 hydrates : Prediction of three phase coexistence line 124505. https://doi.org/10.1063/1.4916119

Muromachi, S., 2021. CO2 capture properties of semiclathrate hydrates formed with tetra-n-butylammonium and tetra-n-butylphosphonium salts from H2 + CO2 mixed gas. Energy 223, 120015. https://doi.org/10.1016/j.energy.2021.120015

Muromachi, S., Abe, T., Maekawa, T., Yamamoto, Y., 2015. Phase equilibrium for clathrate hydrate formed in methane+water+urea system. Fluid Phase Equilib. 398, 1–4. https://doi.org/10.1016/j.fluid.2015.04.007

Naeiji, P., Varaminian, F., Rahmati, M., 2019a. The kinetic modeling of methane hydrate growth by using molecular dynamic simulations. Int. J. Heat Mass Transf. 142, 118356.

https://doi.org/10.1016/j.ijheatmasstransfer.2019.07.006

Naeiji, P., Varaminian, F., Rahmati, M., 2017. Comparison of the thermodynamic, structural and dynamical properties of methane/water and methane/water/hydrate systems using molecular dynamic simulations. J. Nat. Gas Sci. Eng. https://doi.org/10.1016/j.jngse.2017.04.010

Naeiji, P., Varaminian, F., Rahmati, M., 2016. Thermodynamic and structural properties of methane/water systems at the threshold of hydrate formation predicted by molecular dynamic simulations. J. Nat. Gas Sci. Eng. https://doi.org/10.1016/j.jngse.2016.03.044

Naeiji, P., Woo, T.K., Alavi, S., Ripmeester, J.A., 2019b. Molecular dynamic simulations of clathrate hydrate anomalous preservation: The effect of coating clathrate hydrate phases. J. Phys. Chem. C 123, 28715–28725. https://doi.org/10.1021/acs.jpcc.9b07769

P. Steve, C. Paul, T.A., 2012. Large-scale atomic/molecular massively parallel simulator. LAMMPS. Sandia Natl. Labs, Albuquerque, NM.

Phan, A., Schlösser, H., Striolo, A., 2021. Molecular mechanisms by which tetrahydrofuran affects CO2 hydrate growth: Implications for carbon storage. Chem. Eng. J. 129423. https://doi.org/10.1016/j.cej.2021.129423

Rezaei, N., Mohebbi, V., Feyzi, V., 2022. Hybrid hydrate processes for CO2/H2 mixture purification: A techno-economic analysis. Int. J. Hydrogen Energy 47, 10137–10155. https://doi.org/10.1016/j.ijhydene.2022.01.102

Rudolph, A., El-Mohamad, A., McHardy, C., Rauh, C., 2021. Concentrating model solutions and fruit juices using CO2 hydrate technology and its quantitative effect on phenols, carotenoids, vitamin C and betanin. Foods 10, 626. https://doi.org/10.3390/foods10030626

Ryckaert, J.-P., Ciccotti, G., Berendsen, H.J.., 1977. Numerical integration of the cartesian equations of motion of a system with constraints: molecular dynamics of n-alkanes. J. Comput. Phys. 23, 327–341. https://doi.org/10.1016/0021-9991(77)90098-5

Said, S., Govindaraj, V., Herri, J.M., Ouabbas, Y., Khodja, M., Belloum, M., Sangwai, J.S., Nagarajan, R., 2016. A study on the influence of nanofluids on gas hydrate formation kinetics and their potential: Application to the CO2 capture process. J. Nat. Gas Sci. Eng. 32, 95–108. https://doi.org/10.1016/j.jngse.2016.04.003

Saptoro, A., Huo, K.C., 2013. Influences of Indonesian coals on the performance of a coal-fired power plant with an integrated post combustion CO2 removal system: A comparative simulation study. Energy Convers. Manag. 68, 235–243. https://doi.org/10.1016/j.enconman.2013.01.015

Senatore, V., Buonerba, A., Zarra, T., Oliva, G., Belgiorno, V., Boguniewicz-Zablocka, J., Naddeo, V., 2021. Innovative membrane photobioreactor for sustainable CO2 capture and utilization. Chemosphere 273, 129682. https://doi.org/10.1016/j.chemosphere.2021.129682

Sinehbaghizadeh, S., Javanmardi, J., Mohammadi, A.H., 2018. Phase stability conditions of clathrate hydrates in the (methane + 3-methyl-1-butanol + water), (methane + 3,3-dimethyl-2-butanone + water) and (methane + 2,3-dimethyl-2-butene + water) systems: Experimental measurements and thermodynamic modeling. J. Chem. Thermodyn. 125, 64–70. https://doi.org/10.1016/j.jct.2018.05.006

Sinehbaghizadeh, S., Javanmardi, J., Roosta, A., Mohammadi, A.H., 2019a. Estimation of the dissociation conditions and storage capacities of various sH clathrate hydrate systems using effective deterministic frameworks. Fuel 247, 272–286. https://doi.org/10.1016/j.fuel.2019.01.189

Sinehbaghizadeh, S., Javanmardi, J., Roosta, A., Mohammadi, A.H., 2017. A fugacity approach for prediction of phase equilibria of methane clathrate hydrate in structure H. Phys. Chem. Res. 5, 465–481. https://doi.org/10.22036/pcr.2017.69958.1334

Sinehbaghizadeh, S., Roosta, A., Rezaei, N., Ghiasi, M.M., Javanmardi, J., Zendehboudi, S., 2019b. Evaluation of phase equilibrium conditions of clathrate hydrates using connectionist modeling strategies. Fuel 255, 115649. https://doi.org/10.1016/j.fuel.2019.115649

Sinehbaghizadeh, S., Saptoro, A., Amjad-Iranagh, S., Tze Tiong, A.N., Mohammadi, A.H., 2022a. Molecular Dynamics Simulation Studies on the Stability and Dissociation of Clathrate Hydrates of Single and Double Greenhouse Gases. Energy & Fuels 36, 8323–8339. https://doi.org/10.1021/acs.energyfuels.2c01396

Sinehbaghizadeh, S., Saptoro, A., Mohammadi, A.H., 2022b. CO2 hydrate properties and applications: A state of the art. Prog. Energy Combust. Sci. 93, 101026. https://doi.org/10.1016/j.pecs.2022.101026

Sloan, E.D., Koh, C.A., 2008. Clathrate hydrates of natural gases, 3rd Ed. ed. CRC Press, Taylor & Francis Group,

Boca Raton.

Strobel, T.A., Koh, C.A., Sloan, E.D., 2007. Hydrogen storage properties of clathrate hydrate materials. Fluid Phase Equilib. 261, 382–389. https://doi.org/10.1016/j.fluid.2007.07.028

Takeuchi, F., Hiratsuka, M., Ohmura, R., Alavi, S., Sum, A.K., Yasuoka, K., 2013. Water proton configurations in structures I, II, and H clathrate hydrate unit cells. J. Chem. Phys. 138, 124504. https://doi.org/10.1063/1.4795499

Wang, P.-W., Wu, D.T., Lin, S.-T., 2021. Promotion mechanism for the growth of CO2 hydrate with urea using molecular dynamics simulations. Chem. Commun. https://doi.org/10.1039/D0CC06165D

Wu, H., Li, Q., Sheng, M., Wang, Z., Zhao, S., Wang, J., Mao, S., Wang, D., Guo, B., Ye, N., Kang, G., Li, M., Cao, Y., 2021. Membrane technology for CO2 capture: From pilot-scale investigation of two-stage plant to actual system design. J. Memb. Sci. 624, 119137. https://doi.org/10.1016/j.memsci.2021.119137

Xie, N., Tan, C., Yang, S., Liu, Z., 2019. Conceptual design and analysis of a novel CO2 hydrate-based refrigeration system with cold energy storage. ACS Sustain. Chem. Eng. 7, 1502–1511. https://doi.org/10.1021/acssuschemeng.8b05255

Xu, C.G., Yan, R., Fu, J., Zhang, S.H., Yan, K.F., Chen, Z.Y., Xia, Z.M., Li, X. Sen, 2019. Insight into micro-mechanism of hydrate-based methane recovery and carbon dioxide capture from methane-carbon dioxide gas mixtures with thermal characterization. Appl. Energy 239, 57–69. https://doi.org/10.1016/j.apenergy.2019.01.087

Yu, Y.S., Zhou, S.D., Li, X. Sen, Wang, S.L., 2016. Effect of graphite nanoparticles on CO2 hydrate phase equilibrium. Fluid Phase Equilib. 414, 23–28. https://doi.org/10.1016/j.fluid.2015.12.054

Zhang, L., Yang, L., Wang, J., Zhao, J., Dong, H., Yang, M., Liu, Y., Song, Y., 2017. Enhanced CH4 recovery and CO2 storage via thermal stimulation in the CH4/CO2 replacement of methane hydrate. Chem. Eng. J. 308, 40–49. https://doi.org/10.1016/j.cej.2016.09.047

Zhang, P., Tong, J., Huang, K., Zhu, X., Yang, W., 2021. The current status of high temperature electrochemistry-based CO2 transport membranes and reactors for direct CO2 capture and conversion. Prog. Energy Combust.

Sci. 82, 100888. https://doi.org/10.1016/j.pecs.2020.100888

Zhou, S., Yu, Y., Zhao, M., Wang, S., Zhang, G.-Z., 2014. Effect of graphite nanoparticles on promoting CO2 hydrate formation. Energy & Fuels 28, 4694–4698. https://doi.org/10.1021/ef5000886

Zhu, X., Ge, T., Yang, F., Wang, R., 2021. Design of steam-assisted temperature vacuum-swing adsorption processes for efficient CO2 capture from ambient air. Renew. Sustain. Energy Rev. 137, 110651. https://doi.org/10.1016/j.rser.2020.110651

Zuo, X., Zhu, J., An, B., Han, K., Li, R., Wang, E., 2017. Influence of Fe addition on microstructure and properties of Cu-Ag composite. Met. Mater. Int. 23, 974–983. https://doi.org/10.1007/s12540-017-6656-2